Mars Global Surveyor observations of the Halloween 2003 solar superstorm's encounter with Mars

Dana H. Crider,[1] Jared Espley,[2] David A. Brain,[3] David L. Mitchell,[3]
John E. P. Connerney,[4] and Mario H. Acuña[4]

Received 24 October 2004; revised 4 April 2005; accepted 21 April 2005; published 25 August 2005.

[1] Like at Earth, disturbances from solar storms affect the space environment as they encounter Mars. The effects of the 28 October 2003 solar superstorm were among the greatest observed by the Mars Global Surveyor spacecraft at Mars to date. The disturbance, defined by an increase in incident solar wind pressure, encountered Mars on 30 October 2003 and persisted for 43 hours. We present the effects of the passage of this high-pressure disturbance and compare the modified Martian space environment to more quiescent times. We find that the horizontal component of magnetic field is increased on the dayside. In addition, the solar wind interaction region is compressed during the disturbance. The solar wind flow has access to lower altitudes than typical, which likely increases mass loss from the Martian atmosphere. Regions of opened magnetic field lines can be closed at 400 km due to the compression of minimagnetospheres, thus altering locations where ionospheric plasma is protected from solar wind scavenging at 400 km altitude.

Citation: Crider, D. H., J. Espley, D. A. Brain, D. L. Mitchell, J. E. P. Connerney, and M. H. Acuña (2005), Mars Global Surveyor observations of the Halloween 2003 solar superstorm's encounter with Mars, *J. Geophys. Res.*, *110*, A09S21, doi:10.1029/2004JA010881.

1. Introduction

[2] On 28 October 2003, an x-class superflare occurred on the Sun. Energetic particles released during the event bombarded Earth and Mars within a couple of hours. The solar flare was associated with a Coronal Mass Ejection (CME) that released a massive cloud of solar plasma at UT 1030. The parcel of plasma, sometimes called an interplanetary coronal mass ejection (ICME) or a magnetic cloud, traveled from the Sun to Mars in 43–44 hours. Therefore it had an average velocity of 1340 km/s. The ICME had a maximum speed exceeding 2000 km/s when it passed Earth, a velocity consistent with the travel time from the Sun to the Earth [*Skoug et al.*, 2004]. The difference in apparent ICME velocity at Earth and Mars may be attributed to a slowdown occurring after passing Earth orbit. More likely, the difference results from spatial differences in the ICME. The angular separation between Earth and Mars as seen from the Sun was 30° during this event, which translates into 79×10^6 km at Earth orbit and 110×10^6 km at Mars orbit.

[3] Before discussing the data from this storm, first let us describe the regions of the solar wind interaction with Mars as seen from three spacecraft that have taken particles and fields data on it. Of particular interest for this work is the diversion of the solar wind flow around Mars. Phobos 2 observed that the solar wind is typically diverted around Mars at an altitude of around 800–1000 km [*Rosenbauer et al.*, 1989], well above the 400 km mapping orbit of Mars Global Surveyor (MGS). MGS is not equipped with an ion instrument to differentiate between hot solar wind protons and heavy planetary ions. When MGS was in its elliptical orbit, it did provide magnetic field and electron flux evidence of a change in plasma regime at 800–1200 km on the dayside. There, the electron fluxes attenuate, the magnetic field magnitude increases sharply, and turbulence in the magnetic field decreases [*Acuña et al.*, 1998; *Vignes et al.*, 2000]. This was taken to be the lower boundary of the turbulent magnetosheath, or the magnetic pileup boundary (MPB).

[4] Mars Express (MEX) is in an elliptical orbit around Mars. MEX is equipped with ASPERA-3, which includes both ion and electron detectors. It lacks a magnetometer and cannot use magnetic field as a diagnostic. However, the electron detectors on MGS and MEX have an overlapping energy range, both detecting electrons in the 10 eV to 10 keV range. Therefore we can use the electron signature to relate MGS data to MEX data. MEX sometimes measures solar wind ions at altitudes below the altitude at which the electron attenuation is observed [*Lundin et al.*, 2004]. Since the magnetic field signature is always coincident with the electron signature in the MGS data, we can assume that solar wind ions occasionally penetrate the region of piled-up magnetic field below the magnetosheath. The MPB does not

[1]Department of Physics, Catholic University of America, Washington, DC, USA.
[2]Physics and Astronomy, Rice University, Houston, Texas, USA.
[3]Space Science Laboratory, University of California, Berkeley, California, USA.
[4]NASA Goddard Space Flight Center, Greenbelt, Maryland, USA.

0148-0227/05/2004JA010881$09.00

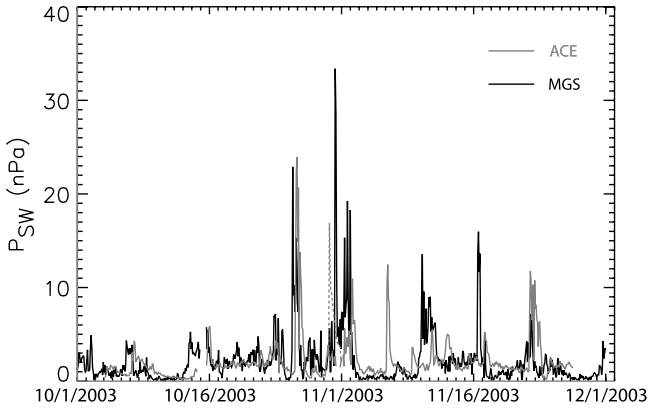

Figure 1. A time series of the solar wind pressure at Mars from October and November 2003. The estimated dynamic pressure from MGS is included as well as the extrapolated solar wind pressure from ACE SWEPAM.

appear to be a hard boundary to the solar wind flow. The solar wind flow is diverted at or below the MPB.

[5] There were two spacecraft in the vicinity of Mars at the time of the Halloween superstorm. Both MGS and Mars Odyssey were in low orbits around Mars. There was no upstream solar wind monitor in the vicinity of Mars. MEX was still en route to Mars, but it was not recording data. MGS is equipped with a Magnetometer/Electron Reflectometer (MAG/ER) experiment package, which measures the vector magnetic field and electron fluxes. Odyssey carries MARIE, which measured the radiation environment at Mars until it was disabled during this event. This report focuses on the effects of the passing ICME on the solar wind interaction with Mars as seen by the MGS MAG/ER.

2. Pressure Increase

[6] An increase in the solar wind dynamic pressure, P_{SW}, accompanies the arrival of an ICME. Although neither MGS nor Odyssey is equipped or positioned correctly to determine the upstream solar wind dynamic pressure, a proxy for P_{SW} can be derived from MAG data. The dominant term in the total pressure changes in the different regions of the solar wind interaction with Mars, but total pressure is conserved in the interaction. In the solar wind, the pressure is dominated by the ram pressure, ρv^2. P_{SW} is converted into thermal pressure, nkT, at the Martian bow shock and into magnetic field pressure, $B^2/2\mu_o$, at the magnetic pileup boundary (MPB). Magnetic pressure dominates at the 400 km MGS altitude. According to Newtonian pressure balance in the flow around a blunt obstacle, the pressure falls off as $\cos^2\theta$, where θ is the angle between the upstream flow velocity direction and the obstacle normal [see, e.g., *Spreiter and Stahara*, 1992]. Fitting this function to the magnetic field data at 400 km altitude on the dayside of Mars, we are able to estimate P_{SW} [*Crider et al.*, 2003]. This proxy is only an approximation because it does not consider possible partitions in the pressure and does not allow the shape of the obstacle to vary. Other models [e.g., *Verigin et al.*, 2004] have done well matching obstacle shape to magnetic field direction. However, our pressure proxy results are strongly correlated with those derived from fitting a function with both a flexible obstacle shape and pressure partition. Because we fit the data from individual orbits, we are only able to resolve P_{SW} on a timescale determined by the orbital period, roughly 2 hours. Changes

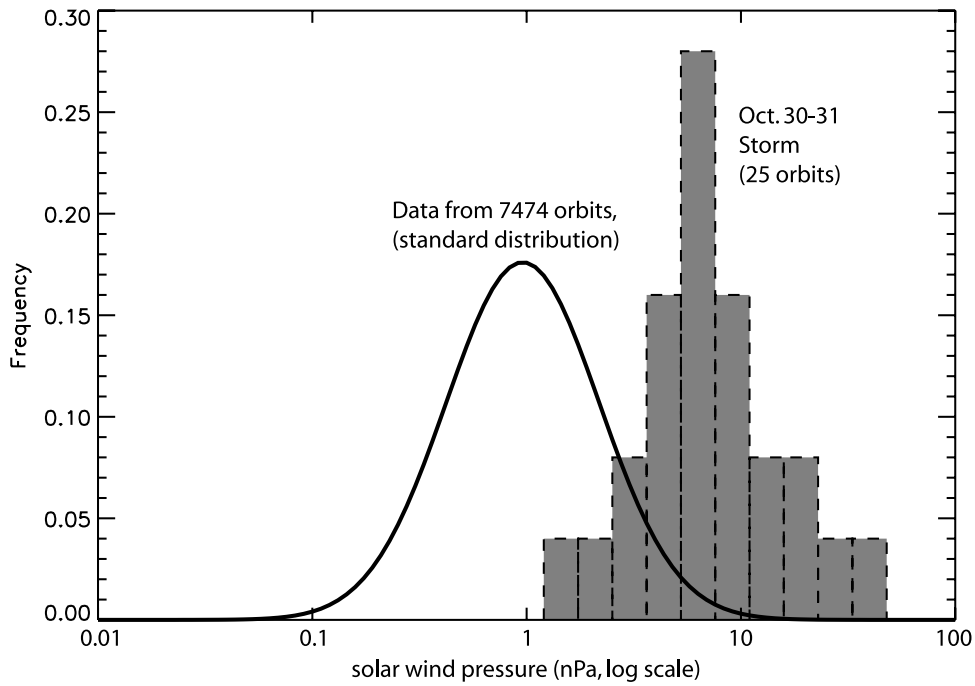

Figure 2. Inferred solar wind pressure distribution from a large group of mapping orbits compared to the orbits from 30–31 October 2003.

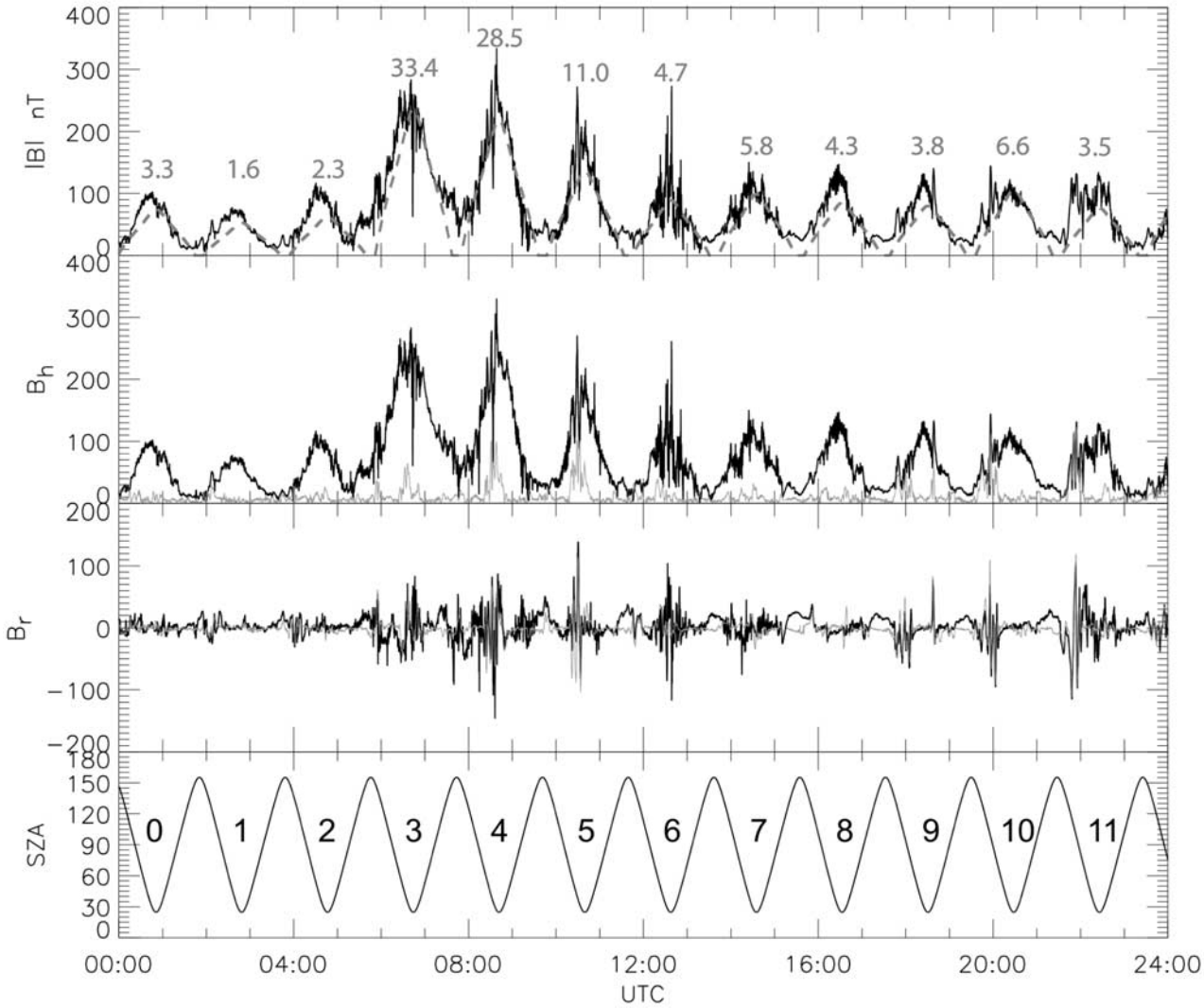

Figure 3. MGS MAG/ER time series data from 30 October 2003. (a) magnetic field magnitude with fit to determine solar wind dynamic pressure (value given at peak of each orbit), (b) horizontal component of B, (c) vertical component of B, and (d) solar zenith angle (with orbit number of the day given).

in the solar wind conditions certainly occur over the period of an MGS orbit and cannot be accounted for here.

[7] Figure 1 shows the time series of the estimated P_{SW} at Mars from October and November of 2003. Also included is P_{SW} calculated from ACE SWEPAM proton density, $\rho_E = m_p n_E$, and velocity, v_E, data taken near Earth [*Skoug et al.*, 2004]. It is extrapolated to Mars' distance from the Sun by assuming the pressure falls off as $1/r^2$:

$$P_M = \rho_E v_E^2 \frac{r_E^2}{r_M^2}, \tag{1}$$

where r_E and r_M are the heliocentric distance of Earth and Mars, respectively. The ACE data are also shifted by time, dt, to account for the travel time of solar wind between Earth orbit and Mars orbit:

$$dt = \frac{(r_M - r_E)}{v_E}. \tag{2}$$

Because we are considering the effects of wide, impulsive events, we do not adjust the time to account for the phase separation of Earth and Mars as we would when comparing solar wind from a persistent source region on the Sun.

[8] First, we note that there are three major events that are observed at both Earth and Mars. They passed Mars on days 26 October, 30–31 October, and 21 November. Note that there is a 23 hour data gap in the ACE density data during the 30–31 October storm. We fill in part of that period with the dotted line when velocity data was available by assuming a constant ρ_E. Because the pressure is proportional to v_E^2, velocity more strongly controls the pressure. Ion velocities are evidence that the storm was indeed very strong as it passed the Earth. There are other events that are only observed at one planet. Some events are stronger at one planet than the other. Earth and Mars are separated by 15°–30° during this time frame. A Spearman rank correlation between the extrapolated ACE data and the MGS proxy gives a $r_s = 0.29$. Comparison of the solar wind, especially an ICME, as it transits from the Earth to Mars is an interesting and worthwhile topic. However, it is not the subject of this paper and will not be discussed further here.

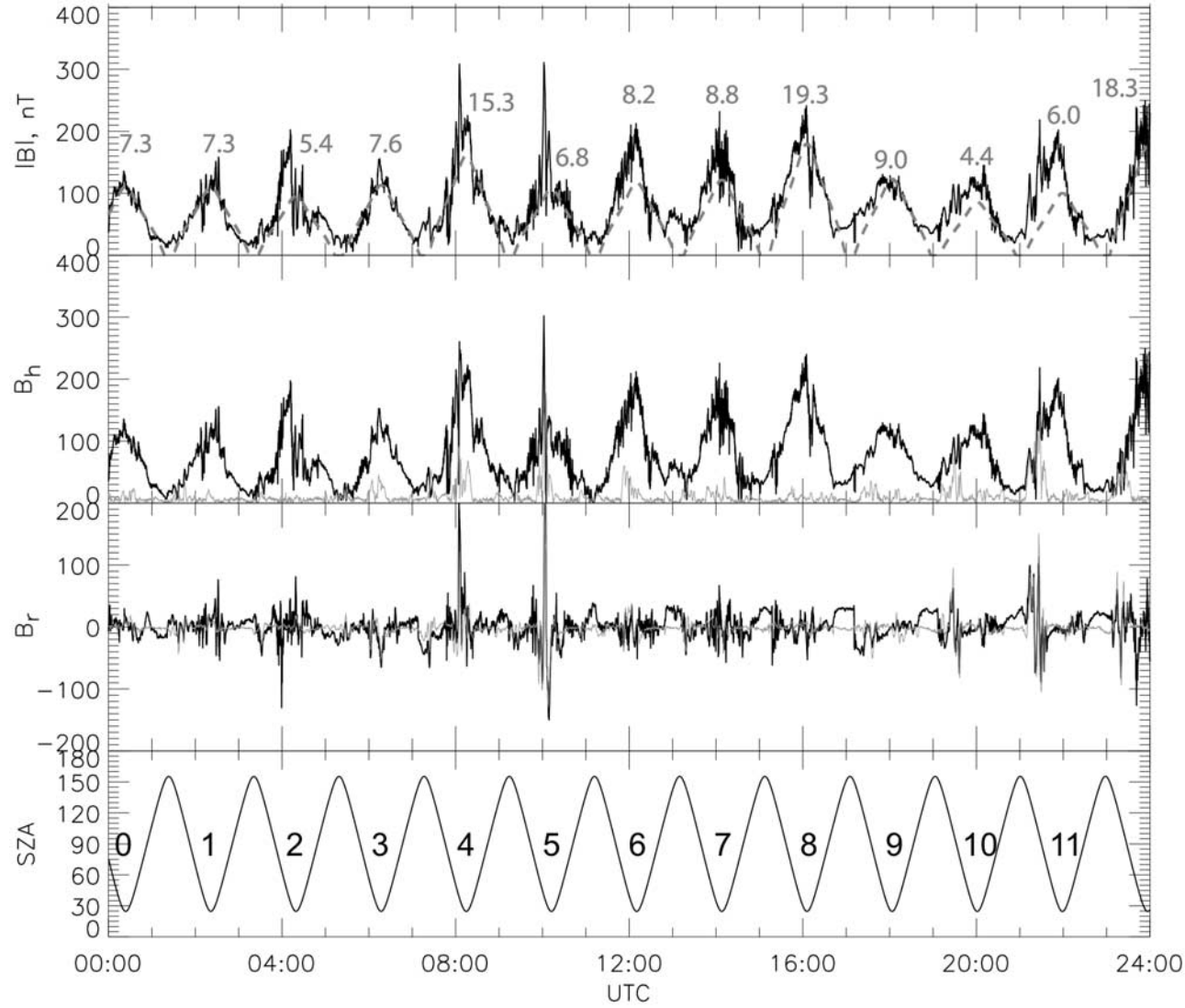

Figure 4. MGS MAG/ER time series data from 31 October 2003. Panels are the same as in Figure 3.

[9] In this paper, we focus on the data from the 30–31 October storm. It exhibits a substantial pressure increase with a duration of almost 2 days. To determine the significance of the observed pressure increase, we look at the typical distribution of P_{SW} at Mars. There is a normal distribution of log P_{SW} when using data over a long time period (see Figure 2). Using this proxy of P_{SW}, the peak of that distribution is just below 1 nPa at Mars. The distribution of P_{SW} from the 25 orbits on 30–31 October 2003 is centered on 6.6 nPa. This storm-time distribution is centered more than 2σ higher than the long-term distribution. The next section presents the MGS MAG/ER data from 30–31 October and interprets the effects of high P_{SW} on the solar wind interaction with Mars.

3. Compression of the Solar Wind Interaction Region

[10] Figures 3 and 4 show the MAG data time series from 30 and 31 October 2003, respectively. Each bottom panel shows the solar zenith angle of the spacecraft. Note that there are 12 orbits in a day. For the purposes of this paper, we consider an orbit to be the period between successive passes through the most antisolar point of the orbit. That way, dayside data on any individual orbit are contiguous. The top panel gives the magnetic field magnitude. The $\cos^2\theta$ fit to the data used to estimate the upstream P_{SW} is superimposed. P_{SW} in nPa is given over each fit. Notable deviations between the data and the fit occur over regions of strong crustal magnetization that affect the local pressure balance and flow geometry. Only data from crustal field free regions of the northern hemisphere obtained on the dayside are used to calculate the best fit, eliminating at least 3/4 of an orbit's data. This becomes obvious on close inspection of the superimposed fit, which fits best for each orbit from the local maximum down to increasing times. The differences on the left side of the maxima (southern hemisphere) are from a combination of temporal variations in P_{SW} and contributions from crustal magnetic sources.

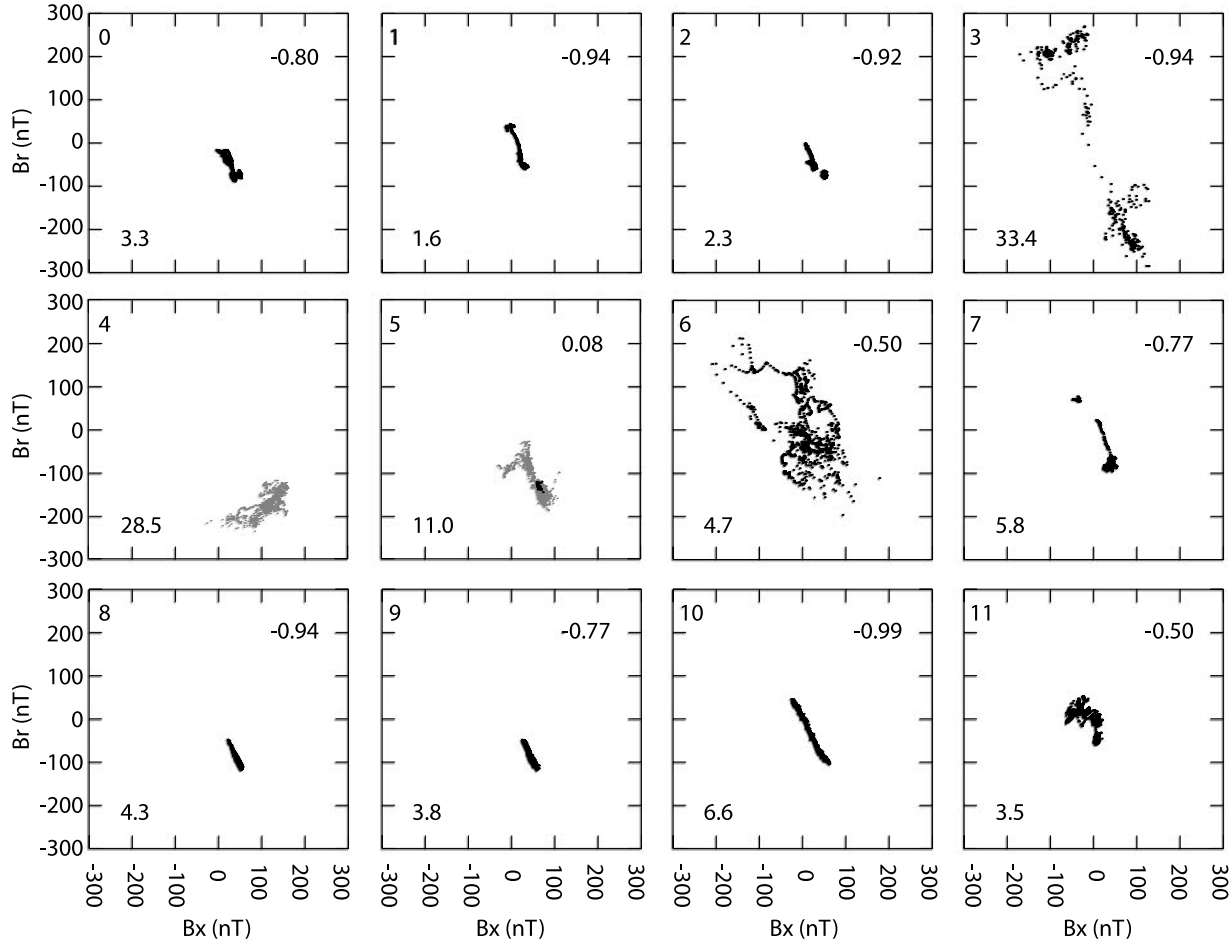

Figure 5. Magnetic field component comparison for the dayside orbits on 30 October 2003. High scatter in this representation is characteristic of the magnetosheath. Orbit numbers in the top left corner of each panel correspond to the orbit numbers in Figure 3. Correlation coefficient to a linear fit appear in the top right corner.

[11] The second and third panels in Figures 3 and 4 show the locally horizontal and vertical components of the magnetic field, respectively. An estimate of the crustal contribution to the magnetic field is given in the second and third panels in orange [*Connerney et al.*, 2001]. The horizontal component increases as the spacecraft moves to lower solar zenith angles and then decreases as the spacecraft goes back to high solar zenith angle on every orbit. This is the large-scale ''draped'' geometry of the induced magnetosphere [*Riedler et al.*, 1989; *Acuña et al.*, 1998; *Crider et al.*, 2004]. In contrast, the largest vertical magnetic fields have a small spatial extent and correspond to crustal sources (e.g., see orbits 4, 5, 9, 10, and 11 on 30 October). Note that the scales of the magnetic field panels are the same. One can see that the increased magnetic pressure comes from an increase in the horizontal component of the magnetic field. These data indicate that there is an increase in the pileup of magnetic field lines during the storm, as is observed under high solar wind pressure at Venus [*Luhmann et al.*, 1980].

3.1. Magnetosheath Observations

[12] Whereas the martian MPB is typically observed at 800–1200 km above the surface, the MPB is pressed down below the 400 km MGS mapping altitude at times during these intense storms. Both magnetic field data and electron data during the storms indicate there are times in which MGS travels through magnetosheath plasma. *Bertucci et al.* [2003] have found that the magnetic field direction is not highly ordered in the hot, turbulent magnetosheath and that it becomes strongly draped around the planet below the magnetosheath in the Magnetic Pileup Region (MPR). Figure 5 shows that the magnetic field direction correlations for the dayside data on 30 October, divided by individual orbit. We use the data from low solar zenith angle (SZA $\leq$ 30°). The analysis utilizes a cylindrical coordinate system in which the Sun-Mars line is the primary axis of the cylinder. The components of magnetic field parallel to the Sun-Mars line and radially away from the Sun-Mars line are compared. We calculated a linear fit for each panel. The correlation coefficient to the fit appears in the top right corner of each panel.

[13] For most passes, there is a strong anticorrelation in the components. This signature is typical in the magnetic pileup region, where magnetic field draping is well defined. A weak correlation between the magnetic field radially outward from the Sun-Mars line and the magnetic field component along the Sun-Mars line in orbits 3, 6, and 11 of the day demonstrates that the spacecraft is located in the

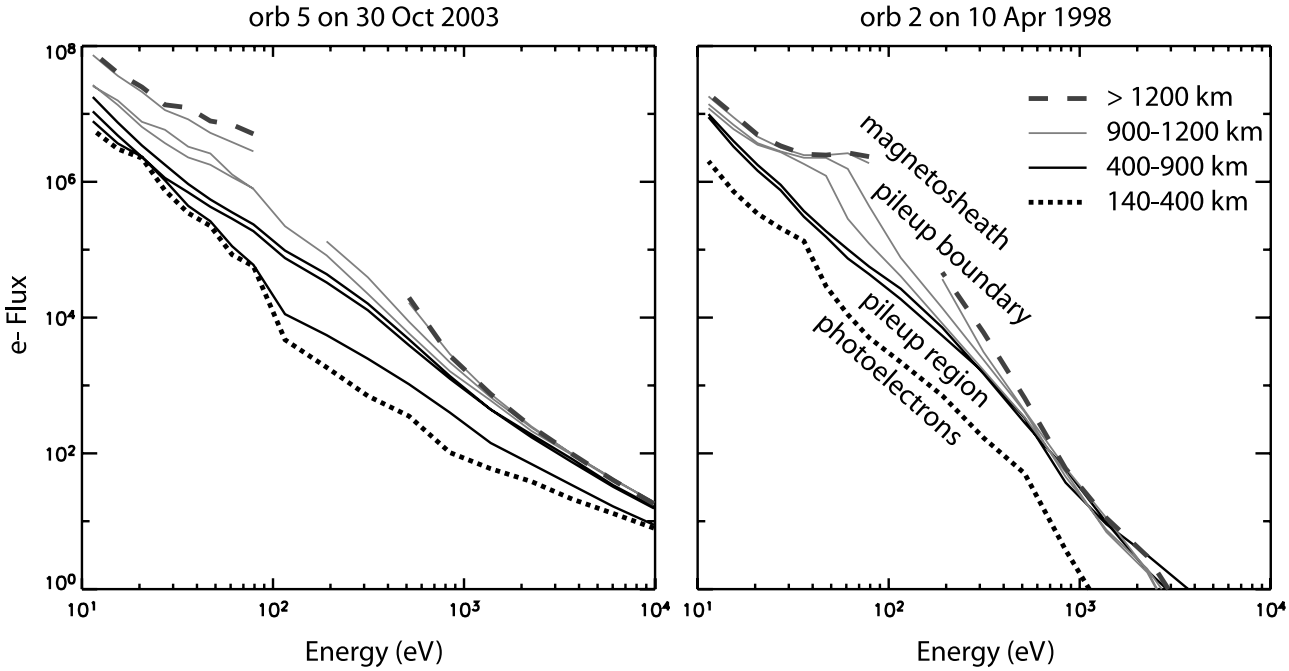

Figure 6. Selected electron spectra from the ER on 30 October 2003 (left) and 10 April 1998 (right). The altitude ranges in which the spectra were observed on 10 April are listed. All the spectra on 30 October were acquired around 400 km. The gaps in the spectra are from channels in which the dead time correction is too great to report the value.

magnetosheath during those dayside passes. The spacecraft was above crustal anomalies, however, while it was at low solar zenith angle during orbits 4 and 5. Although crustal magnetic fields are not typically detectable in the magnetosheath [*Brain et al.*, 2003], given the low altitude of these data, we omitted data from near crustal anomalies for all orbits except 4 and 5. Data taken above crustal fields in orbits 4 and 5 are displayed in gray.

[14] The electron data corroborate this interpretation. Characteristic electron spectra have been identified for the various plasma regions in the solar wind interaction with Mars [*Mitchell et al.*, 2001]. While in an elliptical orbit, ER detected these classes of spectra at certain altitude ranges. Each individual electron spectrum can be used to identify the plasma regime at the spacecraft location. As the interaction region compresses and expands from changing P_{SW}, the altitudes of the plasma regions vary slightly. Figure 6 shows spectra taken during the elliptical orbit phase in the right panel. Solar wind pressure was close to the median value for the orbit on the right side and it is a well studied orbit. The plasma boundaries are located close to the median positions. Typically, photoelectron spectra (dotted line) were observed below 400 km. Magnetosheath spectra (dashed line) were observed above 1200 km. A region of evolving electron spectra marked the bottom of the magnetosheath, typically around 900–1200 km (gray solid line). In the range of 400–900 km, electron spectra of the evacuated magnetic pileup region (black solid line) were typical. The gap in the top magnetosheath spectra at 100 eV is due to an instrumental issue at high electron fluxes. See *Mitchell et al.* [2001] for a more complete description of the ER and dead time correction. For our purposes, it is only important to know that the breaks represent high fluxes in those energy ranges.

[15] During the storm, the spacecraft passes into and out of regions of magnetosheath spectra typically observed at $\geq$900 km (see Figure 6). Thus the magnetic pileup boundary (MPB), or the boundary separating the magnetosheath above from the magnetic pileup region below, is either moving vertically with time or contains spatial variations. The MPB location is known to respond to changes in solar wind pressure [*Verigin et al.*, 1997; *Crider et al.*, 2003] and to the presence of crustal magnetic fields [*Crider et al.*, 2002]. The appearance of magnetosheath spectra at the MGS mapping orbit is a rare occurrence (5–20% of the time, depending on location [*Brain et al.*, 2005]).

[16] All spectra on the left panel are taken from the mapping altitude. That instances of photoelectron spectra, MPR spectra, and magnetosheath spectra are observed indicates spatial and/or temporal fluctuations of the boundaries. As discussed below, complex magnetic field geometry from crustal fields contribute to spatial differences. Solar zenith angle and the slight eccentricity of the spacecraft orbit also account for spatial differences. Temporal differences are the result of temporal fluctuations in the driving forces of the solar wind interaction with Mars, including incident P_{SW}.

[17] Comparing the right and left panels of Figure 6, one notices that the shapes of the spectra are similar. However, the fluxes in the left panel are elevated over typical magnetosheath flux values. This indicates a hotter, denser magnetosheath plasma during the passage of the storms. Also, because the fluxes are elevated, there are more energy bins in which the dead time correction was too great. That is

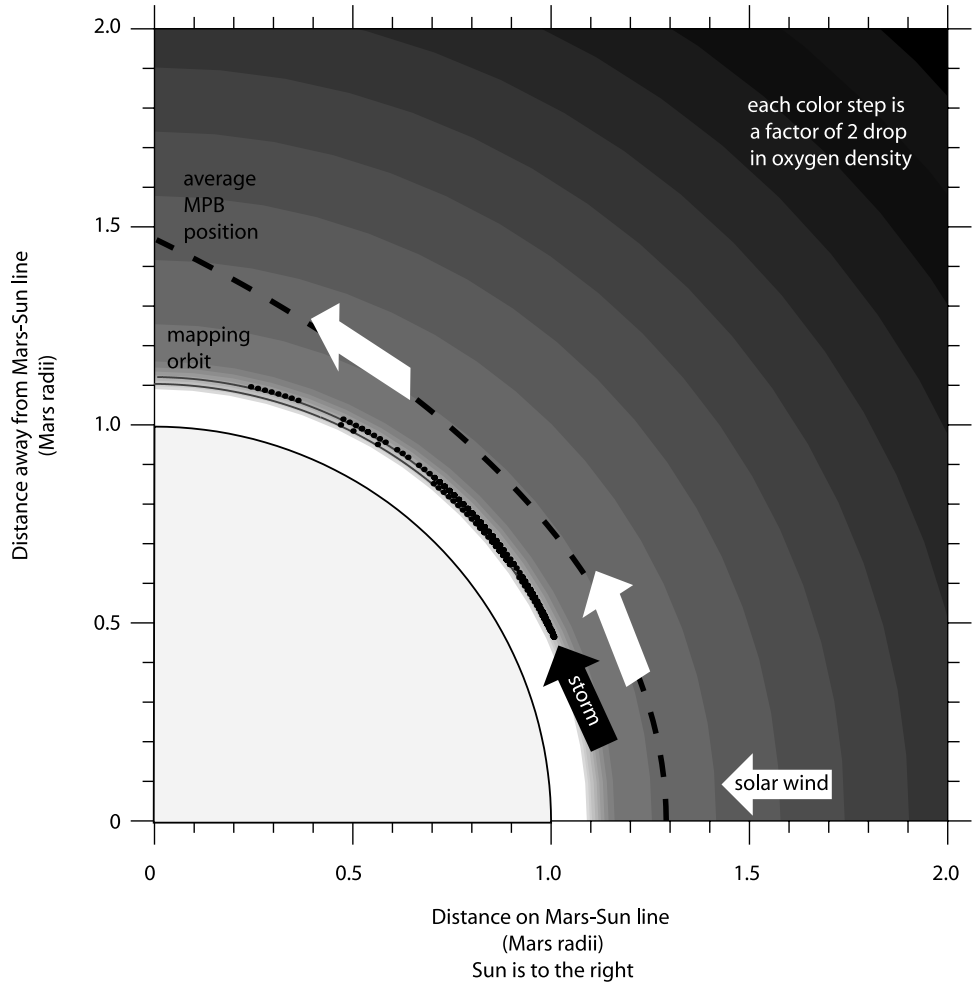

Figure 7. Location of magnetosheath spectra in cylindrical coordinates. The shading shows the exospheric O density. The mean location of the MPB is also shown for reference.

why the gaps in the spectra cover a larger energy range than in the right panel.

[18] Although we can not determine the depth to which the hot, shocked solar wind penetrated before being diverted around Mars during this storm because MGS was fixed at 400 km altitude, these data confirm that the solar wind penetrated to at least 400 km and therefore reached much denser depths of the exosphere than typical. In Figure 7, we indicate the locations of magnetosheath spectra with black spots. The orbital trajectory is also shown. For reference, the black dashed line displays the average location of the lower boundary of the magnetosheath [*Vignes et al.*, 2000]. These data are superposed on a contour plot of exospheric oxygen density at Mars [*Kim et al.*, 1998]. The exospheric oxygen density is a factor of 50 greater at 400 km than at 900 km. Exospheric hydrogen is 2.5 times denser there [*Nagy et al.*, 1990].

[19] There are several processes that contribute to atmospheric loss at Mars, including charge exchange, electron impact ionization, Jeans' escape, and sputtering [see, e.g., *Luhmann and Bauer*, 1992]. Because charge exchange and electron impact ionization are linearly related to neutral density, these ion production rates are accordingly increased by the solar wind's excursion to low altitude during the storm. Some of these pickup ions escape from the Mars system, resulting in an increase in the atmospheric erosion during the storm. Other heavy ions are driven back into the Martian atmosphere. The reimpacting ions sputter neutrals from the atmosphere, an additional loss process [*Luhmann and Kozyra*, 1991]. The loss rate realized from sputtering is a function of the incident ion flux and energy. A particle simulation would be required to quantify the loss rate under storm-time conditions. Although the impacting ion flux is certainly increased during the storm, the excess ions are produced at low altitude. Therefore they do not experience much acceleration before reaching the atmosphere. Perhaps data from MEX will provide insight into loss processes from Mars both during quiescent and storm-time conditions.

3.2. Minimagnetospheres

[20] Spectra consistent with locally produced photoelectrons are typical in the region from 170 to 400 km altitude (170 km is the lowest altitude from which the ER obtained data). When the ER detects this spectrum, it means that the spacecraft is on a magnetic field line that does not have access to the solar wind. Therefore the field line is either embedded in the planet's ionosphere or a closed magnetic field line of planetary origin. The high-altitude limit of this

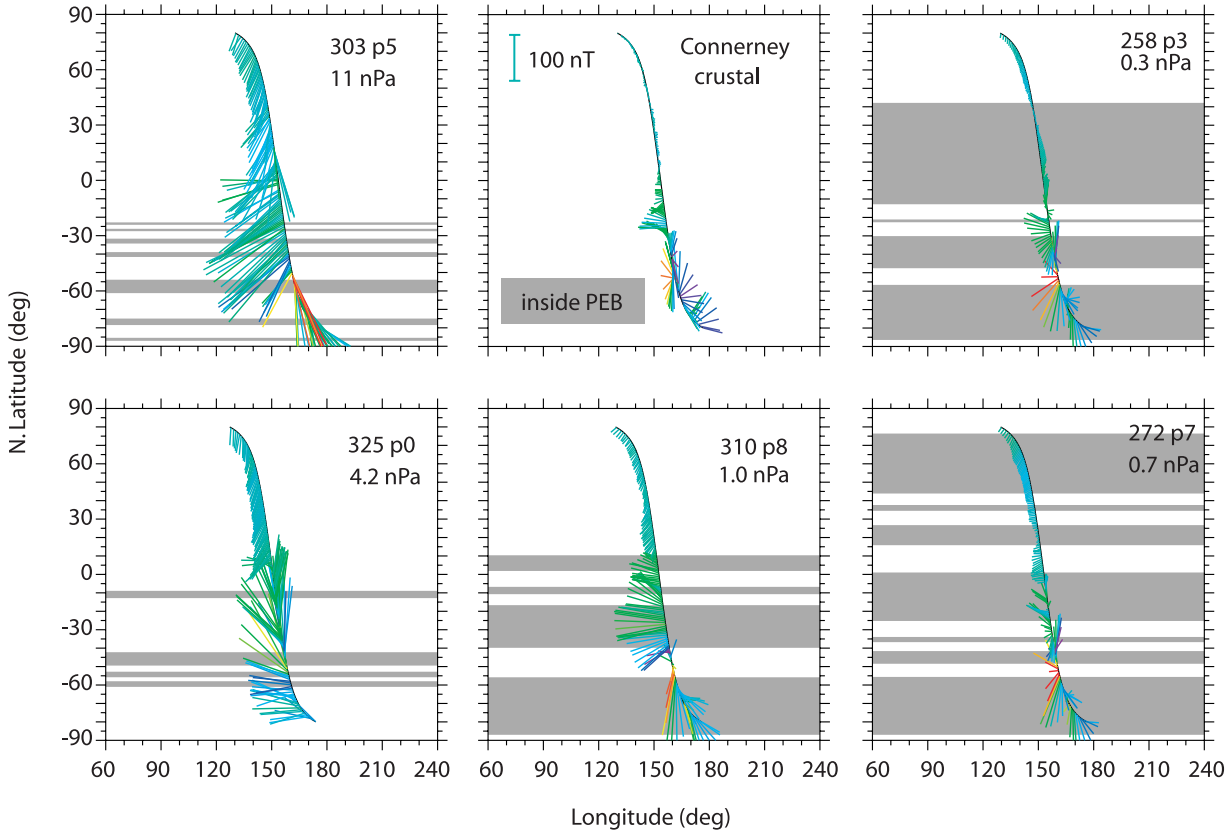

Figure 8. Magnetic field vectors for five orbits with similar ground tracks but different incident solar wind pressure.

region is called the "photoelectron boundary" (PEB) by *Mitchell et al.* [2001]. They show that the altitude of the PEB moves in response to magnetic field geometry of crustal magnetic fields, solar wind pressure, solar EUV flux, and solar zenith angle. During the 30–31 October storm, relatively few photoelectron spectra are observed. The increased P_{SW} depresses the PEB to below spacecraft altitude during much of 30–31 October 2003. Therefore the solar wind electrons have access to 400 km throughout most of the passing storm.

[21] Interestingly, the few locations where photoelectron spectra are detected correspond to regions that typically have strong radial magnetic fields [*Connerney et al.*, 2001]. These locations are often magnetic cusps. In Figure 8, we compare data from several different passes over the same ground track (same local time, altitude, planetary latitude and longitude) with the solar wind magnetic field draped around the dayside northern hemisphere in a similar direction. However, P_{SW} does vary for the selected orbits and decreases counterclockwise from the top left panel. The top center panel shows the magnetic field vectors from *Connerney et al.* [2001]. This top center panel effectively represents the contribution of magnetic fields emanating from the planet's crust to the magnetic field measurements. The vector magnitude and direction give the components parallel to the planet surface. The color code denotes the value of the radial component, with blue indicating downward pointing magnetic field and red indicating outward pointing. The color of the scale vector in the top center panel shows the 0 color for the radial component. The magnitude of the draped magnetic field is highest under high solar wind pressure. As shown in Figure 3, the increased magnetic field occurs in the horizontal component, not radial component.

[22] The gray horizontal bars are drawn in at latitudes where photoelectron spectra are observed. As P_{SW} increases, less of the orbit is under the PEB. The region from 50 to 55°S is a magnetic cusp. The magnetic field has a large positive radial component and it is a small window in which no photoelectron spectra are observed. The cusp can be seen to shrink in width in Figure 8 as the solar wind pressure increases.

[23] Furthermore, the regions adjacent to the cusp are among the few regions below the PEB in the two storm cases (left panels). The high solar wind pressure increases the locally horizontal component of the magnetic field and enables the closure of some planetary field lines. Photoelectrons on these closed minimagnetosphere field lines are isolated from the solar wind unlike most other positions at spacecraft altitude during high pressure. This is in contrast to the broad regions of photoelectron spectra under low P_{SW}. In those cases, the entire ionosphere stands up higher. IMF lines are imbedded in the ionosphere and solar wind electrons are no longer observed on them.

4. Conclusion

[24] Data from MGS MAG/ER indicate that the effect of high incident solar wind dynamic pressure at Mars is the general compression of the interaction region [*Verigin et al.*,

1997; *Crider et al.*, 2003]. The shocked solar wind has access to very low altitudes during the Halloween 2003 solar storm. There it encounters the dense, lower exosphere and ionosphere of Mars. Solar wind protons and electrons interact strongly with atmospheric neutrals through charge exchange and electron impact ionization [*Breus et al.*, 1989; *Holmstrom et al.*, 2002; *Crider et al.*, 2000]. These reaction rates are drastically increased because of the hotter, denser nature of the passing disturbance and the increased neutral density at the altitude to which the solar wind penetrates. This leads to increased atmospheric erosion during the event. Although the steady state solar wind interaction with Mars is not sufficient to account for the loss of water from the inventory of Mars over the last 3.5 billion years [*Lammer et al.*, 1996; *Crider*, 1999], events such as these are significant to the total solar wind erosion of the atmosphere.

[25] The exact depth of solar wind penetration can not be determined with this data. However, if there is another large solar storm directed at Mars during Mars Express' lifetime at Mars, we hope to be able to observe the details of the solar wind penetration into the martian atmosphere/ionosphere. Together with sophisticated modeling of the interaction, we can use observations of extreme conditions like those in October/November 2003 to better understand the effects of the solar wind interaction on the evolution of the martian atmosphere.

[26] **Acknowledgments.** This work was performed under NASA grant NAG5-12235. ACE SWEPAM data provided courtesy of the ACE SWEPAM team and NASA ACE Science Data Center.

[27] Arthur Richmond thanks David Mitchell and Mikhail Verigin for their assistance in evaluating this paper.

References

Acuña, M. H., et al. (1998), Magnetic field and plasma observations at Mars: Initial results of the Mars Global Surveyor mission, *Science*, *279*, 1676–1680.

Bertucci, C., et al. (2003), Magnetic field draping enhancement at the Martian magnetic pileup boundary from Mars Global Surveyor observations, *Geophys. Res. Lett.*, *30*(2), 1099, doi:10.1029/2002GL015713.

Brain, D. A., F. Bagenal, M. H. Acuña, and J. E. P. Connerney (2003), Martian magnetic morphology: Contributions from the solar wind and crust, *J. Geophys. Res.*, *108*(A12), 1424, doi:10.1029/2002JA009482.

Brain, D. A., J. S. Halekas, R. Lillis, D. L. Mitchell, R. P. Lin, and D. H. Crider (2005), Variability of the altitude of the martian sheath, submitted to *Geophys. Res. Lett*.

Breus, T. K., S. J. Bauer, A. M. Krymskii, and V. Y. Mitnitskii (1989), Mass loading in the solar wind interaction with Venus and Mars, *J. Geophys. Res.*, *94*, 2375–2382.

Connerney, J. E. P., M. H. Acuña, P. J. Wasilewski, G. Kletetschka, N. F. Ness, H. Rème, R. P. Lin, and D. L. Mitchell (2001), The global magnetic field of Mars and implications for crustal evolution, *Geophys. Res. Lett.*, *28*, 4015–4018.

Crider, D. (1999), Evidence of electron impact ionization in the magnetic pileup boundary of Mars–Observations and modeling results, Ph.D. thesis, Rice Univ., Houston, Tex.

Crider, D., et al. (2000), Evidence of electron impact ionization in the magnetic pileup boundary of Mars, *Geophys. Res. Lett.*, *27*, 45–47.

Crider, D. H., et al. (2002), Observations of the latitude dependence of the location of the martian magnetic pileup boundary, *Geophys. Res. Lett.*, *29*(8), 1170, doi:10.1029/2001GL013860.

Crider, D. H., D. Vignes, A. M. Krymskii, T. K. Breus, N. F. Ness, D. L. Mitchell, J. A. Slavin, and M. H. Acuña (2003), A proxy for determining solar wind dynamic pressure at Mars using Mars Global Surveyor data, *J. Geophys. Res.*, *108*(A12), 1461, doi:10.1029/2003JA009875.

Crider, D. H., D. A. Brain, M. H. Acuna, D. Vignes, C. Mazelle, and C. Bertucci (2004), Mars Global Surveyor observations of solar wind magnetic field draping around Mars, *Space Sci. Rev.*, *111*(1-2), 203–211.

Holmström, M., S. Barabash, and E. Kallio (2002), Energetic neutral atoms at Mars: 1. Imaging of solar wind protons, *J. Geophys. Res.*, *107*(A10), 1277, doi:10.1029/2001JA000325.

Kim, J., A. F. Nagy, J. L. Fox, and T. E. Cravens (1998), Solar cycle variability of hot oxygen atoms at Mars, *J. Geophys. Res.*, *103*, 29,339–29,342.

Lammer, H., W. Stumpter, and S. Bauer (1996), Loss of H and O from Mars: Implications for the planetary water inventory, *Geophys. Res. Lett.*, *23*, 3353–3365.

Luhmann, J. G., and S. J. Bauer (1992), Solar wind effects on atmosphere evolution at Venus and Mars, in *Venus and Mars: Atmospheres, Ionospheres, and Solar Wind Interactions*, *Geophys. Monogr. Ser.*, vol. 66, edited by J. G. Luhmann, M. Tatrallyay, and R. O. Pepin, pp. 417–430, AGU, Washington, D. C.

Luhmann, J. G., and J. U. Kozyra (1991), Dayside pickup oxygen ion precipitation at Venus and Mars: Spatial distributions, energy deposition, and consequences, *J. Geophys. Res.*, *96*, 5457–5467.

Luhmann, J. G., R. C. Elphic, C. T. Russell, J. D. Mihalov, and J. H. Wolfe (1980), Observations of large scale steady magnetic fields in the dayside Venus ionosphere, *Geophys. Res. Lett.*, *7*, 917–920.

Lundin, R., et al. (2004), Solar wind-induced atmospheric erosion at Mars: First results from ASPERA-3 on Mars Express, *Science*, *305*, 1933–1936.

Mitchell, D. L., R. P. Lin, C. Mazelle, H. Rème, P. A. Cloutier, J. E. P. Connerney, M. H. Acuña, and N. F. Ness (2001), Probing Mars' crustal magnetic field and ionosphere with the MGS electron reflectometer, *J. Geophys. Res.*, *106*, 23,418–23,427.

Nagy, A. F., J. Kim, and T. E. Cravens (1990), Hot hydrogen and oxygen in the upper atmosphere of Venus and Mars, *Ann. Geophys.*, *8*, 251–256.

Riedler, W., K. Schwingenschuh, D. Moehlmann, V. N. Oraevskii, E. Eroshenko, and J. Slavin (1989), Magnetic fields near Mars - First results, *Nature*, *341*, 604–607.

Rosenbauer, H., N. Shutte, A. Galeev, K. Gringauz, and I. Apathy (1989), Ions of Martian origin and plasma sheet in the Martian magnetosphere - Initial results of the TAUS experiment, *Nature*, *341*, 612–614.

Skoug, R. M., J. T. Gosling, J. T. Steinberg, D. J. McComas, C. W. Smith, N. F. Ness, Q. Hu, and L. F. Burlaga (2004), Extremely high speed solar wind: 29–30 October 2003, *J. Geophys. Res.*, *109*, A09102, doi:10.1029/2004JA010494.

Spreiter, J. R., and S. S. Stahara (1992), Computer modeling of the solar wind interaction with Venus and Mars, in *Venus and Mars: Atmospheres, Ionospheres, and Solar Wind Interactions*, *Geophys. Monogr. Ser.*, vol. 66, edited by J. G. Luhmann, M. Tatrallyay, and R. O. Pepin, pp. 345–383, AGU, Washington, D. C.

Verigin, M., et al. (1997), Quantitative model of the Martian magnetopause shape and its variation with the solar wind ram pressure based on Phobos 2 observations, *J. Geophys. Res.*, *102*(A2), 2147–2155.

Verigin, M., D. Vignes, D. Crider, J. Slavin, M. Acuña, G. Kotova, and A. Remizov (2004), Martian obstacle and bow shock: Origins of boundaries anisotropy, *Adv. Space Res.*, *33*(12), 2222–2227, doi:10.1016/S0273-1177 (03)00522-2.

Vignes, D., et al. (2000), The solar wind interaction with Mars: Locations and shapes of the bow shock and the magnetic pile-up boundary from the observations of the MAG/ER experiment onboard Mars Global Surveyor, *Geophys. Res. Lett.*, *27*, 49–52.

M. Acuña and J. Connerney, NASA Goddard Space Flight Center, Greenbelt, MD 20771, USA.

D. Brain and D. Mitchell, Space Sciences Laboratory, University of California, Berkeley, CA 94720, USA.

D. H. Crider, Department of Physics, Catholic University of America, 106 Driftwood Drive, Gibsonville, NC 27249, USA. (crider@cua.edu)

J. Espley, Physics and Astronomy, Rice University, Houston, TX 77005, USA.